

Segmentation of Major Temporal Arcade in Angiography Images of Retina Using Generalized Hough Transform and Graph Analysis

Farshad Nabi¹

Hamed Yousefi¹

Hamid Soltanian-Zadeh,^{1,2} *Senior Member, IEEE*

¹ CIPCE, School of Electrical and Computer Engineering, College of Engineering, University of Tehran, Tehran, Iran

² Image Analysis Laboratory, Radiology Department, Henry Ford Health System, Detroit, Michigan, USA

Abstract—Structural analysis of the vascular architecture of the retina facilitates the diagnosis of retinopathy because retinopathy affects the blood flow velocity. To this end, blood flow velocity in the major temporal arcade (MTA) vessel in retina may be measured to detect blood flow velocity changes. For this measurement, separation of the MTA vessel is a necessary step. We propose methods for identifying the MTA vessel. We use Gabor filters to detect retinal vessels and Hough transform to model the MTA vessel. Then, we use the MTA model to find a seed point for image segmentation. Next, we take advantage of graph theory to track temporal arcade vessels and separate the MTA vessel. We have evaluated our algorithm using 43 clinical angiography images, in which traces of MTA was drawn by an ophthalmologist. Experimental results show that the proposed methods correctly separate MTA in 93%.

Keywords—Blood vessels; angiography images; Gabor filters; Hough transform; retinopathy; major temporal arcade.

I. INTRODUCTION

A. Diabetic Retinopathy

Diabetic Retinopathy (DR) is one of an epidemic disease of the human visual system caused by the increase of the glucose level in the blood vessels. In addition, this disease is responsible for early blindness of patients younger than 70 years in developed countries [1]. Statistics indicate that the risk of blindness in diabetic patients is 25 times more than the healthy subjects [2]. In the past, it was believed that structural changes such as hemorrhages and presence of red lesions in the eye are the first symptoms of DR and as a result, the disease was not detected before visual loss and total impairment of the visual acuity. Most of the methods for prevention and treatment of diabetic retinopathy are based on retinal morphological variations such as micro aneurysms and exudates [3], [4], [5]. Nevertheless, a recent procedure has spotted DR by looking at the functional variations that happen before structural variations. To this end, blood flow velocity variations that occur before any other morphological changes have been evaluated [6].

The blood flow velocity is higher in patients with early diabetes mellitus than the healthy subjects. This is due to the increase of the blood glucose for a long duration of time that impresses structure and function of blood vessels wall.

B. Major Temporal Arcade Modeling

Detection of the major temporal arcade (MTA) is useful for the measurement of the blood flow velocity and localization of the optic nerve head and fovea [6]. The major temporal arcade may be identified by applying Hough transform [6] on the segmented vessels.

Niemeijer et al. [7] used a point distribution model to represent the major temporal arcade, where they used a set of 10 points to mark MTA. They used five hundred images to minimize a cost function and estimate the model parameters. The cost function included two global terms, width and orientation of the vessels, and one local term, anatomic measurements around the model points. The optimization was done in both of the image and parameter spaces. The estimated parameters were used to generate a point distribution model of MTA. A human observer may check how many of the ten points lie correctly on MTA. Niemeijer et al. [7] reported 93.2% complete detection of MTA, 5.6% partial detection, and 1.2% complete failure to detect MTA in 500 images of the retina. Fleming et al. [8] used vessel enhancement and semielliptical curve fitting using the generalized Hough transform to model MTA. After enhancing the vessels and obtaining an edge map of the vessels, the generalized Hough Transform was applied to skeletonized image of the vasculature. The Global maxima in the Hough transform domain was chosen as the best match for the MTA model.

C. Identifying and Tracking Vessels

Retinal vessel extraction involves segmentation of the vascular structure and identification of distinct vessels by linking the segments of the vascular structure [9].

Lau et al. [9] used a graph model for the segmented vascular structure and formulated the problem of identifying vessels as the problem of finding the optimal forest in the graph under a set of constraints.

The previous methods of modeling MTA, explained in Section I-B, do not practically extract the MTA vessel. Furthermore, the coordinates of the center of the optic disc are used as a vertex of the temporal arcade angle. In this paper, we present a method to extract and separate MTA using Gabor filters, generalized Hough transform, and optimal tree.

II. METHODS

A. Preprocessing

The proposed methods were tested with angiography images of the retina from the Feiz Hospital in Isfahan, Iran. These images were taken using a Heidelberg Retina Angiograph 2 (HRA2) system, which is a confocal laser scanning system for digital fluorescent and indocyanine green angiography. The laser, included in HRA2, diffuses a laser light for fluorescent angiography with 488 nm wavelength. Recently, a video capture device was added to the HRA2 apparatus. Since typical enhancement methods are not appropriate for extracting the vessels from the retina in the angiography images [10], [11], we applied the Gabor transform followed by a Laplacian of Gaussian (LoG) filter [12]. Next, we extracted the retinal blood vessels using a statistical local thresholding (SLT) approach.

Laplacian is a second isotropic derivative of the image, which is used to find regions with fast intensity changes (edge detection). Since the second derivative is very sensitive to noise, we reduced the noise using a Gaussian filter. Applying these two operators to an image is named LoG, which is:

$$L_{\sigma}(p; \sigma) = (\nabla^2 M(n; \sigma)) * I(n) \quad (1)$$

where ∇^2 is the Laplacian operator, $M(n, \sigma)$ is an isotropic zero mean Gaussian kernel, and σ^2 is the kernel's variance. The symbol “*” stands for the convolution operation and I is the grayscale format of the input image. Finally, the image was convolved with the LoG filter and the output was thresholded to obtain the largest values in the image:

$$L(p) = \max_{\sigma} L_{\sigma}(p; \sigma) \quad (2)$$

In order to improve the image contrast, we applied a Gabor wavelet filter to the image, which is defined by a sinusoidal component multiplied by a Gaussian kernel as:

$$B(p; \lambda, \alpha, \theta) = s(p; \lambda) M(p; \alpha, \theta) \quad (3)$$

where $s(\cdot)$ is the sinusoidal component and $M(\cdot)$ is an anisotropic, scaled, and rotated Gaussian function. We applied the filter with different wavelength (λ), scale (α), and orientation (θ). The maximum response was obtained by varying (λ), (α), and (θ) as:

$$G(p) = \max_{\lambda, \alpha, \theta} (L(p) * B(p; \lambda, \alpha, \theta)) \quad (4)$$

Fig. 1 shows the results of the image enhancement step.

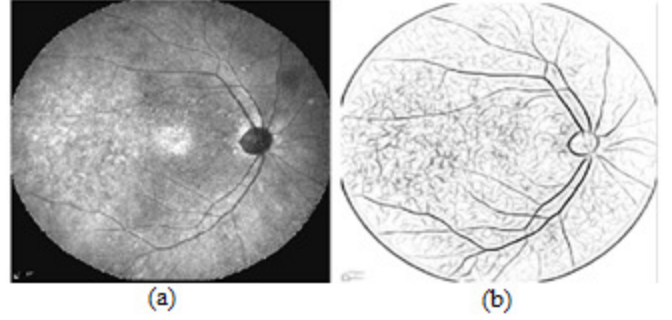


Figure 1. (a) angiography image, (b) Output of the Gabor filter followed by the LoG filter.

Some errors occur in the vessel extraction step owing to the fact that the image background is not uniform. However, SLT provides improvement by dividing the image into non-overlapping rectangles based on their non-uniformly distributed intensity. SLT is defined as:

$$T_{xy} = a \cdot m_{xy} \quad (5)$$

An 11×11 window was considered for each pixel and the mean intensity was calculated by:

$$m_{xy} = \frac{1}{11^2} \sum_{x=-5}^{x+5} \sum_{y=-5}^{y+5} I(x, y) \quad (6)$$

where m_{xy} is the mean intensity in the selected window, $I(x, y)$ is the image intensity. The constant a in (5) is used to adjust the accuracy of vessel extraction based on the noise variations and vessels accretion.

Next, the image is segmented as:

$$g(x, y) = \begin{cases} 0 & I(x, y) > T_{xy} \\ 1 & I(x, y) \leq T_{xy} \end{cases} \quad (7)$$

In (7), 0 is considered for background and 1 is considered for the vessels.

Fig. 2 Shows the result of applying SLT to a angiography image.

B. Hough Transform

Hough [13] proposed an approach to find lines in an image. Hough transform has been generalized to detect other parameterized curves like parabolas [14], [15], [16], [17]. Here, we define a parabola with its directrix parallel to the y -axis and its symmetrical axis parallel to the x -axis as follows:

$$(y - y_0)^2 = 4a(x - x_0)^2 \quad (8)$$

where $(x - x_0)$ is the vertex of model and the quantity $4a$ is the latus rectum. The quantity of a defines the aperture of the parabola and indicates the alignment of the opening of the parabola; for a positive value, the parabola opens to the right. The parameters (x_0, y_0, a) define the Hough space. Every non-zero pixel in the image corresponds to a parabola in the Hough

space for each value of a . Each point in the Hough space expresses a parabola in the image domain. The size of (x_0, y_0) planes in the Hough space is equal to the size of the image (768×868). The value of a is restricted by physiological limits on the arcade and the size of the image. For our database, the value of a was in the range of $[30, 60]$. We assumed that only positive values of a were defined. For images that the opening of temporal arcade was toward left, it was rotated by 180° so the arcade would open to the right.

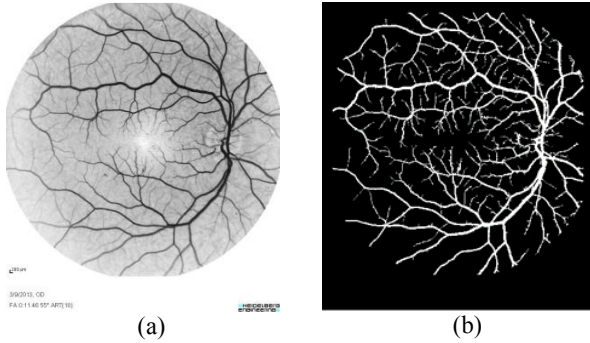


Figure 2. (a) An angiography image, (b) Output of the SLT algorithm.

We applied the above, generalized Hough transform to the vessel map images. The point with highest value in the Hough space was used to model the parabola for MTA. This model was used to track and separate the MTA vessel.

C. Graph-Based Description of Vessel Map Image

In this section, we define our graph-based description of the vessel map images obtained from the above preprocessing step. We mask the optic disc for the graph creation approach, because of irregular and highly tortuous blood vessels at this region. The mask window is a circle with radius of $2r$, where r is the radius of optic disc. Masking the optic disc like this is used in a number of clinical studies [18], [19]. Each vessel starts from a root point that is near the circle of radius $2r$. These root points are denoted in red in Fig. 3(b).

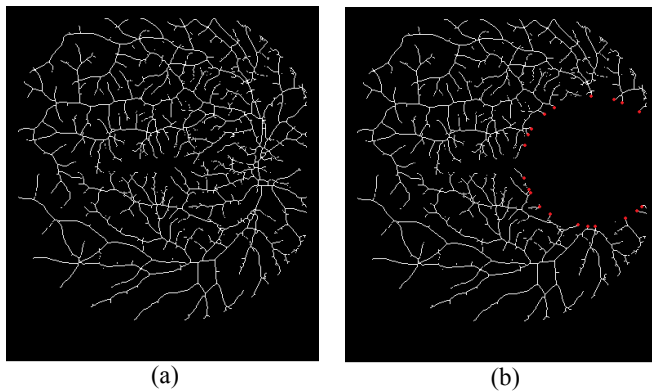


Figure 3. (a) A skeletonized vessel map image, (b) Masked image with root points denoted in red.

Next, we find the root points corresponding to the MTA vessel using the Hough Transform model obtained in Section I.B. As the parabola model is more correlative with MTA near the optic disc, we used the distance $2r$ (from the center of optic disc) to find the corresponding root point. The distance $2r$ is optimal because as it is neither too close to the optic disc, which is the origin of all vessels, nor too far, where the MTA vessel and parabola model diverge. We found the closest root point to the parabola model and kept it as the start seed for the graph tree creation [20]. Now, having the root points corresponding to MTA, we should track the true MTA. Our aim is to identify the MTA vessel and represent it in the form of a binary tree. Vessels in a retinal image frequently cross each other and bifurcate. That makes MTA tracking a challenge.

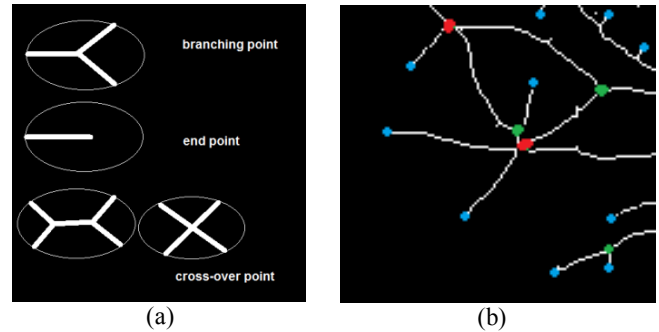


Figure 4. (a) Landmark points classification, (b) Landmark points plotted on a part of the vessel map image. End points are denoted in blue, cross-over points in red, and branching points in green.

We used a depth first search (DFS) approach to track all vessel trees, and find all branching points, cross-over points, and end points. The algorithm searches for three types of landmark point by analyzing the 3×3 neighborhood of foreground pixels such that the pixels with one foreground neighbor are defined as end points, the pixels with three foreground neighbors are defined as branching points, and two foreground pixels close to each other and each one with three foreground neighbors or the foreground pixel with four or more foreground neighbors are defined as cross-over points. Fig. 4 shows how landmark points are classified.

We used a circular window centered at the candidate point to find the landmark points in the vessel map image. The diameter of this window is set according to the maximum vessel diameter expected in the vessel map image. In order to validate and classify the landmark points, we applied a zero-cross detector along the circumference of the window. Landmark points are classified according to the number of zero-crossings.

- 1) It is end point, if we have one zero-crossing
- 2) It is branching point, if we have three zero-crossings
- 3) It is cross-over, if we have more than three zero-crossings or if we have two branching points very close to each other, which can lie inside the circular window.

Next, we identify vessel segments between two branching/crossing (B/C) points or those between a B/C point and an end point, in the skeletonized vessel map. A DFS approach traverses skeletal vessel segments to identify vessel line segments. We reconstruct the corresponding vessel segment for each skeletal line segment to obtain the features of that segment. We extract three features from the two end regions of each reconstructed vessel segment: 1) Segment orientation, 2) Segment diameter, and 3) Segment intensity.

These features are used to form a cost function in the graph description of the vessel segments. In the graph presentation, each vessel segment is represented by a node, and the cost between two neighboring vessel segments is represented by a cost edge.

Fig. 5(a) shows skeletal vessel segments. Fig. 5(b) shows reconstructed vessel segments. Fig. 5(c) shows three vessel segments in red, green, and yellow with end region of each segment in blue. Fig. 5(d) shows the corresponding graph representation for Fig. 5(c) with edge costs between the nodes. Fig. 5(e) shows a vessel with root segment (segments connected to the root points are considered as root segments) denoted in red, end points in yellow, and other segments in blue. Fig. 5(f) shows the corresponding graph representation for Fig. 5(e). The segments with an end point in Fig. 5(f) are represented by a yellow node.

Starting from root points of MTA, we just need to find the shortest path to the end points. We have two root points, in the upper half of the vessel image and in the lower half, corresponding to the MTA vessel. Dijkstra's algorithm is used to find the shortest path. Shortest path is the path with smallest sum of costs over the total path. The algorithm starts from the root segment and propagates till it reaches the end points and enlists their corresponding cost path values. The path with the smallest cost path is chosen as the MTA vessel. The algorithm is repeated for the rest of MTA vessel inside the circle of radius $2r$ but here the end point is the segment of a vessel with the center of optic disc on it. The whole procedure is summarized in Fig. 6.

III. EXPERIMENTAL RESULTS

Fig. 7(a) shows one of the original images of our database. Fig. 7(b) shows the result of applying Log and Gabor wavelet filtering to improve the contrast of the image. Fig. 7(c) shows the result of applying SLT, in order to create a binary image and segment vessels. In Fig. 7(d) after applying generalized Hough transform to the vessel map image, the parabola with the highest value is obtained for $\alpha = 56$; this parabola model is drawn on the vessel map image in green. We use this parabola model to find the root points, on the circle of radius $2r$, corresponding to the MTA vessel. The closest root points to the parabola model are considered as root points of MTA vessel, and denoted as red dots.

Fig. 7(e) shows the part of MTA vessel obtained from applying the Dijkstra's algorithm to the graph description of the vessel segments. Here, the vessel segments inside the

circle of radius $2r$ are masked. Dijkstra starts from the two root points and continues till it reaches the end of vessels.

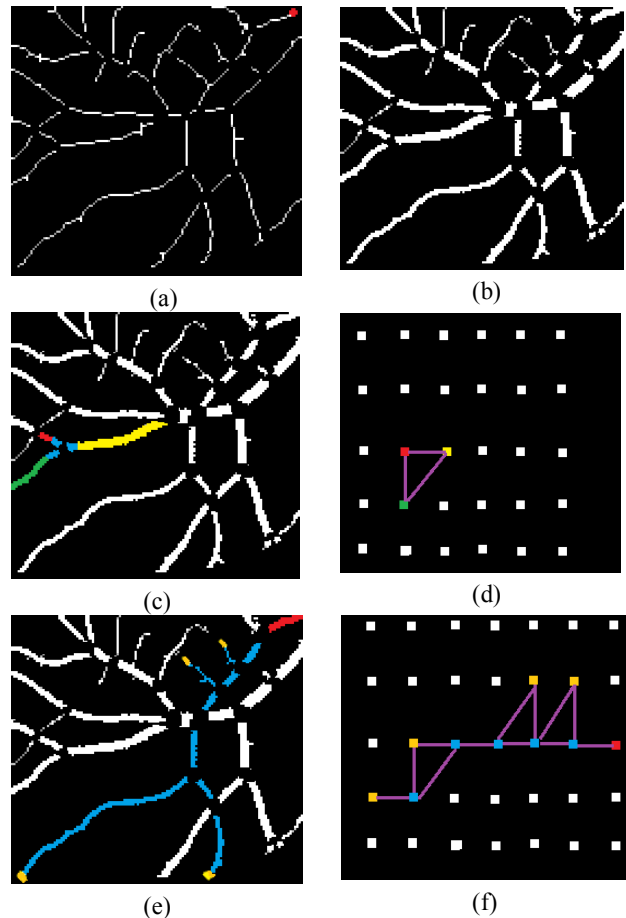


Figure 5. Obtaining the graph description for vessels, (a) skeletal vessel segments, (b) reconstructed vessel segments, (c) three vessel segments in red, green, and yellow with end region of each segment in blue, (d) the corresponding graph representation for Fig. 5(c) with edge costs between nodes, (e) a vessel with root segment (segments connected to the root points are considered as root segments) denoted in red, end points in yellow, and other segments in blue, (f) the corresponding graph representation for Fig. 5(e). The segments with an end point in Fig. 5(f) are represented by a yellow node.

In Fig. 7(f), vessel segments outside the circle of radius $2r$ are masked. The Dijkstra's algorithm starts from the same root points but ends in the center of the optic disc. Fig. 7(g) shows the MTA vessel obtained from the vessels in Fig. 6(e) and Fig. 6(f). The result of MTA separation using the Hough transform and optimal tree applied to 43 angiography images of the Feiz Hospital database, indicated 40 correct separation, and 3 wrong separation. MTA vessels were drawn by an ophthalmology expert. We compared the hand drawn MTAs with the extracted MTAs using the XOR operator:

$$T = H \otimes E \quad (12)$$

where H is the binary hand drawn image of MTA, and E is the extracted MTA image. Next, we calculated the portion of number of ones in T to the number of the image pixels:

$$P = \frac{\sum T}{N} \quad (13)$$

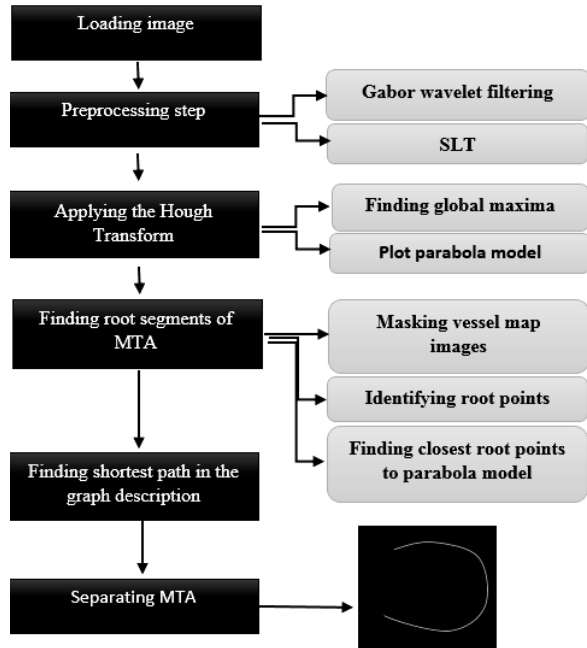


Figure 6. Block diagram of the proposed method.

where N is number of pixels in the image. Then, depending on the value of P , we decided to consider the extracted MTA as correct or as incorrect separation:

$$\begin{cases} P \leq 0.01 & \text{correct separation} \\ P > 0.01 & \text{incorrect separation} \end{cases} \quad (14)$$

In previous works, the authors have just calculated a model for MTA without practically extracting the MTA vessel. The MTA model is beneficial, but in some applications like blood flow velocity computation, we need to have the MTA vessel. In [10], Niemeijer et al. introduced a point distribution model, which fitted to the vascular arc of the image. In [9], Oloumi et al. used the Hough transform to model MTA but they did not go further to extract the MTA vessel itself. In [11], Fleming et al. used vessel enhancement and semielliptical curve fitting using the generalized Hough transform to model MTA.

In our approach, we take advantages of obtained model and the Generalized Hough-Transform to track MTA itself.

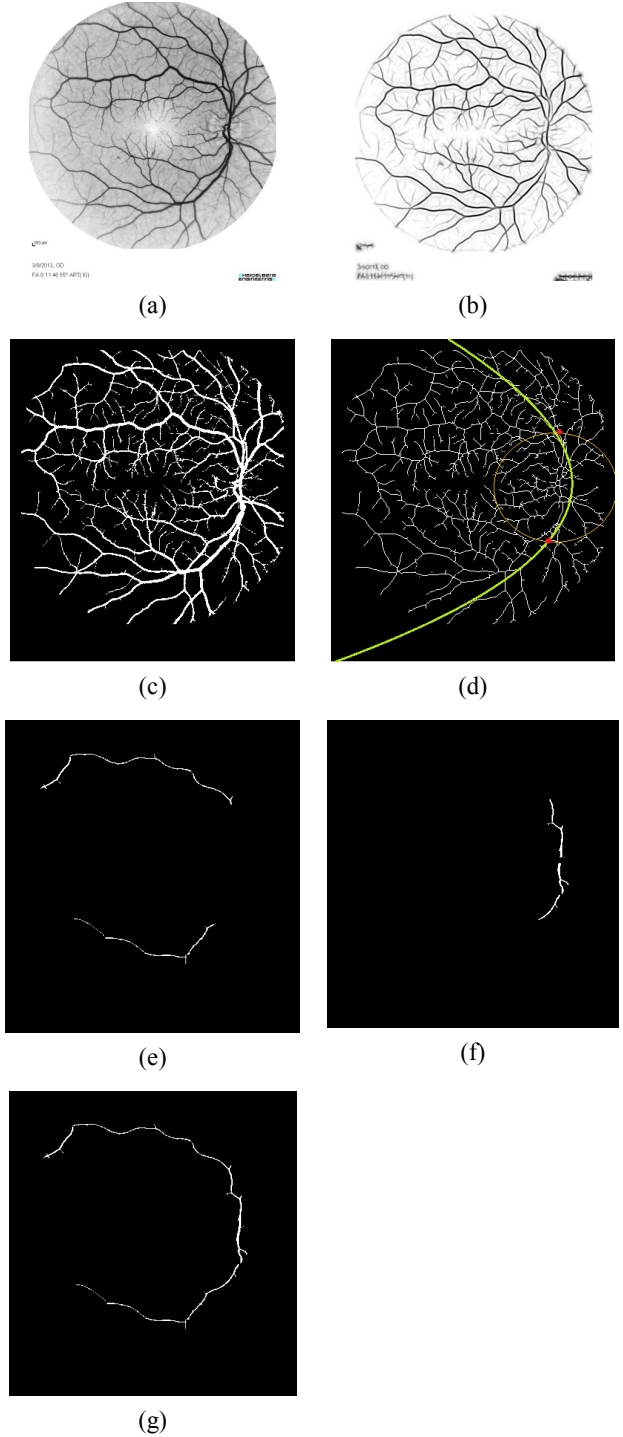


Figure 7. (a) One of the original images of our database. (b) Original image after preprocessing including LoG and Gabor wavelet filtering. (c) The extracted vessel using SLT. (d) Finding closest root points (denoted in red dots) to the parabola model (drawn in green color). (e) Shortest paths outside the circle of radius $2r$. (f) Shortest paths inside the circle of radius $2r$. (g) MTA vessel.

IV. DISCUSSION AND CONCLUSION

Using the SLT approach for the thresholding of the Gabor wavelet response is more sensitive to find minor vessels than fixed thresholding. We can use fixed thresholding to prevent the detection of minor vessels. Pruned vessel maps generate a superior fitted parabola, and consequently it is more likely that a correct MTA is extracted. Beside acceptable results of this work, there are some limitations that need to be addressed. Finding the correct initial component at the beginning is very dependent on the fitness of the parabola model to MTA. If we could use a cost function to consider other features like the thickness of the connected components, then we could have a more accurate and robust MTA detection algorithm.

In this work, we took advantage of the graph theory to track the MTA vessel in addition to defining a model using the Hough transform.

The proposed method was successful in separating the MTA vessel from the angiography images of the retina. The extracted MTA can be used in the blood flow velocity calculation of the angiography videos; it is beneficial for the diagnosis and therapy of retinopathy.

ACKNOWLEDGMENT

The authors thank Dr. Mohammadreza Akhlaqi for his scientific guidance and the Feiz Hospital in Isfahan, Iran, for providing the angiography images of the retina.

REFERENCES

- [1] R. Klein, B. E. Klein, "Vision disorders in diabetes", *Diabetes in America*, vol. 1, pp. 293-338, 1995.
- [2] Centers for disease control and prevention (CDC), "Public health focus: prevention of blindness associated with diabetic retinopathy", *MMWR Morb Mortal Wkly Rep*, 19;42(10):191-195, 1993.
- [3] S. N. Shajahan, R. C. Roy, "An Improved Retinal Blood Vessel Segmentation Algorithm based on Multi-structure Elements Morphology", *I. J. Computer Applications*, vol. 57, pp. 8875 – 8887, 2012.
- [4] M. Kalaivani, M. S. Jeyalakshmi, V. Apama, "Extraction Of Retinal Blood Vessels Using Curvelet Transform And Kirsch's Templates", *I. J. Emerging Technology and Advanced Engineering*, vol. 2, pp. 2450-2459, 2012.
- [5] L. Zhou, M. S. Rzeszutarski, L. J. Singerman, and J. M. Chokreff, "The detection and quantification of retinopathy using digital angiograms", *IEEE Trans. Med. Imag.*, vol. 13, pp. 619–626, 1994.
- [6] F. Oloumi, and R.M.Rangayyan, "Detection of the Temporal Arcade in Fundus Images of the Retina Using the Hough Transform", *International Conference of the IEEE EMBS*, vol. , pp. 3585-3588, september. 2009.
- [7] M. Niemeijer, M. D. Abràmoff, and B. van Ginneken, "Segmentation of the optic disk, macula and vascular arch in fundus photographs," *IEEE Trans. Med. Imag.*, vol. 26, no. 1, pp. 116–127, Jan. 2007.
- [8] A. D. Fleming, K. A. Goatman, S. Philip, J. A. Olson, and P. F. Sharp, "Automatic detection of retinal anatomy to assist diabetic retinopathy screening," *Phys. Med. Biol.*, vol. 52, no. 2, pp. 331–345, Jan. 2007.
- [9] Q. P. Lau, M. L. Lee, W. Hsu, and T. Y. Wong, "Simultaneously Identifying All True Vessels From Segmented Retinal Images," *IEEE transactions on biomedical engineering*, vol. 60, no. 7, pp 1851–1858, July 2013.
- [10] J. L. Starck, F. Murtagh, E. J. Candes, and D. L. Donoho, "Gray and color image contrast enhancement by the curvelet transform", *Image Processing*, *IEEE Trans*, vol. 12, pp. 706-717, 2003.
- [11] T. Acharya and A. Ray, *Image Processing: Principles and Applications*, Wiley-Interscience, 2005.
- [12] R. Estrada, C. Tomasi, M. T. Cabrera, D. K. Wallace, S. F. Freedman, and S. Farsiu, "Exploratory Dijkstra forest based automatic vessel segmentation: applications in video indirect ophthalmoscopy (VIO)", *Biomed optics express*, vol. 3, pp. 327-338, 2012.
- [13] Hough PVC, "Method and means for recognizing complex patterns," *US Patent 3, 069, 654*, December 18, 1962.
- [14] Rangayyan RM, *Biomedical Image Analysis*, CRC, Boca Raton, FL, 2005.
- [15] Jafri MZM and Deravi F, "Efficient algorithm for the detection of parabolic curves," *Vision Geometry III*, vol. 2356, pp. 53–62, 1994.
- [16] Ballard DH, "Generalizing the Hough transform to detect arbitrary shapes," *Pattern Recognition*, vol. 13, no. 2, pp. 111–122, 1981.
- [17] Wechsler H and Sklansky J, "Finding the rib cage in chest radiographs," *Pattern Recognition*, vol. 9, no. 1, pp. 21–30, 1977.
- [18] C. Y.-L. Cheung, Y. Zheng, W. Hsu, M. L. Lee, Q. P. Lau, P. Mitchell, J. J. Wang, R. Klein, and T. Y. Wong, "Retinal vascular tortuosity, blood pressure, and cardiovascular risk factors," *Ophthalmology*, vol. 118, pp. 812–818, 2011.
- [19] C. Y.-L. Cheung, W. T. Tay, P. Mitchell, J. J. Wang, W. Hsu, M. L. Lee, Q. P. Lau, A. L. Zhu, R. Klein, S. M. Saw, and T. Y. Wong, "Quantitative and qualitative retinal microvascular characteristics and blood pressure," *J. Hypertens*, vol. 29, no. 7, pp. 1380–1391, 2011.
- [20] S. Rattathanapad, B. Uyyanonvara, P. Mittrapiyanuruk, p. Kaewtrakulpong, "Vessel Segmentation in Retinal Images using Graph-Theoretical Vessel Tracking", *IAPR Conference on Machine Vision Applications*, pp. 548_551, 2011